The HCN domain is required for HCN channel cell-surface expression and couples voltage- and cAMP-dependent gating mechanisms

Received for publication, March 1, 2020, and in revised form, April 23, 2020 Published, Papers in Press, April 27, 2020, DOI 10.1074/jbc.RA120.013281

Ze-Jun Wang[1], **Ismary Blanco**[2], **Sebastien Hayoz**[1], **and Tinatin I. Brelidze**[1,2,*]

From the [1]*Department of Pharmacology and Physiology and the* [2]*Interdisciplinary Program in Neuroscience, Georgetown University Medical Center, Washington, D. C., USA*

Edited by Mike Shipston

Hyperpolarization-activated cyclic nucleotide-gated (HCN) channels are major regulators of synaptic plasticity and rhythmic activity in the heart and brain. Opening of HCN channels requires membrane hyperpolarization and is further facilitated by intracellular cyclic nucleotides (cNMPs). In HCN channels, membrane hyperpolarization is sensed by the membrane-spanning voltage sensor domain (VSD), and the cNMP-dependent gating is mediated by the intracellular cyclic nucleotide-binding domain (CNBD) connected to the pore-forming S6 transmembrane segment via the C-linker. Previous functional analysis of HCN channels has suggested a direct or allosteric coupling between the voltage- and cNMP-dependent activation mechanisms. However, the specifics of this coupling remain unclear. The first cryo-EM structure of an HCN1 channel revealed that a novel structural element, dubbed the HCN domain (HCND), forms a direct structural link between the VSD and C-linker–CNBD. In this study, we investigated the functional significance of the HCND. Deletion of the HCND prevented surface expression of HCN2 channels. Based on the HCN1 structure analysis, we identified Arg^{237} and Gly^{239} residues on the S2 of the VSD that form direct interactions with Ile^{135} on the HCND. Disrupting these interactions abolished HCN2 currents. We also identified three residues on the C-linker–CNBD (Glu^{478}, Gln^{482}, and His^{559}) that form direct interactions with residues Arg^{154} and Ser^{158} on the HCND. Disrupting these interactions affected both voltage- and cAMP-dependent gating of HCN2 channels. These findings indicate that the HCND is necessary for the cell-surface expression of HCN channels and provides a functional link between voltage- and cAMP-dependent mechanisms of HCN channel gating.

Hyperpolarization-activated cyclic nucleotide-modulated (HCN) channels are peculiar members of the voltage-gated potassium channel superfamily. Unlike other potassium channels, which are depolarization-activated and highly selective for K^+, HCN channels are activated by membrane hyperpolarization and permeate both Na^+ and K^+ (1, 2). The opening of HCN channels is further facilitated by cyclic nucleotides (1–3). Because of these unique features, HCN channels serve as pacemakers that regulate rhythmic firing of neurons and cardiomyocytes (4–6). HCN channels also have a variety of other functions, including the regulation of membrane resting potential and synaptic transmission (4). In mammals, the HCN channel family contains four isoforms (HCN1–HCN4). All four isoforms are expressed in the brain, where they generate hyperpolarization-activated currents (I_h) (1, 7). Mutations in HCN1 and HCN2 channels had been linked to genetic epilepsy in humans (8–12). HCN4 channels are the predominant isoform in the heart, where they generate hyperpolarization-activated inward currents known as the "funny current" (I_f) (13, 14). Genetically occurring mutations in HCN4 channels are linked to sick sinus syndrome and bradycardias in humans (15, 16).

Similar to other potassium channels, HCN channels are assembled from four subunits, with each subunit containing six transmembrane segments (S1–S6). S1–S4 form a voltage-sensing domain (VSD), and S5 and S6, together with the pore-forming P-loop between them, form the pore domain (PD) of the channels (4, 17). In their intracellular C-terminal regions, HCN channels contain cyclic nucleotide-binding domain (CNBD) linked to the S6 segment with the C-linker (Fig. 1*A*) (17, 18). The VSD is responsible for the hyperpolarization-dependent opening of the channel, and the CNBD enables HCN channels to bind cyclic nucleotides and regulate membrane excitability in response to the changes in the cellular cyclic nucleotide levels (1–3). It has been suggested that the voltage-dependent and cyclic nucleotide–dependent activation mechanisms are coupled. For instance, the K381E mutation in the VSD increases the effect of cAMP on HCN2 currents ~10-fold (19). Simultaneous recording of HCN2 channel currents and changes in the fluorescence of a fluorescent cAMP analog upon binding to the channels revealed that the membrane hyperpolarization enhances the cAMP affinity of the channel activation (20). Finally, a computational analysis of the voltage- and cAMP-dependent activation of HCN2 channels indicated that cAMP binding alters the voltage-dependent gating of HCN2 channels (21). Despite the evidence, the molecular nature of the structural and functional coupling between the VSD and CNBD is unclear.

Recent cryo-EM structure of HCN1 channels identified a novel N-terminal structural motif formed by a stretch of 45 amino acids directly preceding the S1 transmembrane segment (Fig. 1, *A* and *B*, *orange*) (17). The novel motif, called HCN domain (HCND), consists of three α-helices (HCNa, HCNb,

* For correspondence: Tinatin I. Brelidze, tib5@georgetown.edu.
Present address for Sebastien Hayoz: Division of Biology and Biological Engineering, California Institute of Technology, Pasadena, California, USA.

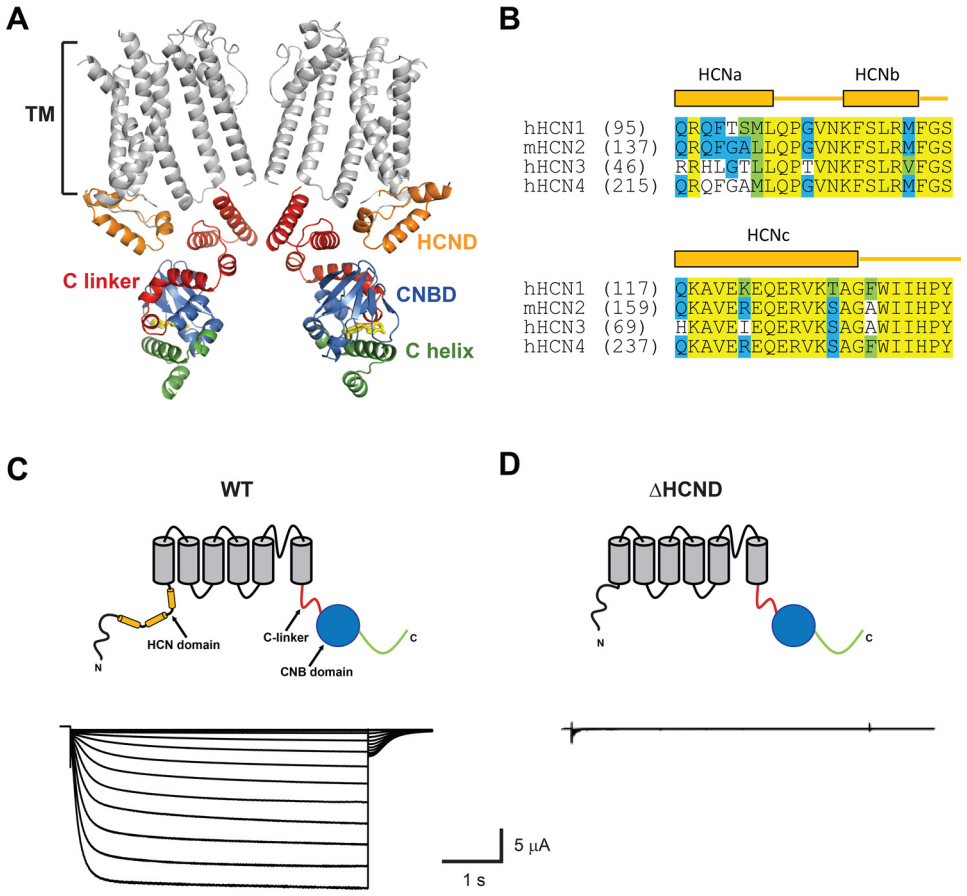

Figure 1. HCND is required for the function of HCN2 channels. *A*, ribbon representation of the cryo-EM structure of HCN1 (PDB code 5U6P; Ref. 17). Only two diagonal subunits are shown for clarity. The transmembrane segments (*TM*) are *gray*, the HCND is *orange*, the C-linker is *red*, the CNBD is *blue*, and the distal C terminus is *green*. cAMP is shown in *yellow*. *B*, amino acid sequence alignment of the HCND for all four mammalian HCN channel isoforms. Identical residues are shown on a *yellow background*, conserved residues are on a *blue background*, and similar residues are on a *green background*. *Letters* without a background indicate nonsimilar residues. *C* and *D*, representative currents recorded from the WT (*C*) and ΔHCND mutant (*D*) mHCN2 channels.

and HCNc) and is conserved in all four HCN channel isoforms. Located on the periphery, the HCND forms direct interactions with the VSD and, also, the C-linker–CNBD (Fig. 1*A*). In this study, we investigated the role of the HCND in the function of HCN channels by using a combination of mutagenesis, membrane surface biotinylation assay, and analysis of HCN2 channel currents recorded from excised inside-out membrane patches and with the two-electrode voltage-clamp (TEVC) technique. In the final stages of our investigation, Porro *et al.* (22) published a study on the role of the HCND in HCN channel gating. Although the main findings of this study are similar to ours, most of the interacting residues investigated by Porro *et al.* differ from the ones described here. These differences are highlighted throughout the manuscript.

We found that the deletion of the HCND completely abolished currents from HCN2 channels by decreasing the surface expression of the channels. Similarly, disruption of the interactions between the S2 of the VSD and HCND abolished HCN2 currents. Disruption of the interactions between the C-linker–CNBD and HCND affected voltage-dependent gating, cAMP sensitivity, and kinetics of deactivation of HCN2 channels. These results indicate that the HCND is necessary for the expression of functional HCN channels, and it functionally links the VSD and CNBD in HCN2 channels. Preliminary results have appeared in abstract form (23).

Results

Deletion of the HCND abolishes currents from HCN2 channels

To investigate the importance of the HCND for the function of HCN2 channels, we generated ΔHCND mutant channels lacking the HCND (deletion of residues 137–180). The WT and ΔHCND mutant HCN2 channels were expressed in *Xenopus laevis* oocytes, and currents were recorded using the TEVC technique. Although the WT channels gave rise to currents with characteristic hyperpolarization-dependent activation (Fig. 1*C*), ΔHCND mutant channels did not show any hyperpolarization-activated currents (Fig. 1*D*). The absence of hyperpolarization-activated currents was observed in $n \geq 60$ independent experiments, performed on oocytes from different batches. These results suggest that the HCND is necessary for the function of HCN channels.

Deletion of the HCND dramatically decreased surface expression of HCN2 channels

To test whether the HCND is necessary for the surface expression of HCN2 channels, we performed surface biotinylation assay on HEK293 cells transfected with the WT and ΔHCND mutant HCN2 channels. In addition, we used untransfected HEK293 cells as a negative control. For these experiments proteins expressed at the membrane surface were bioti-

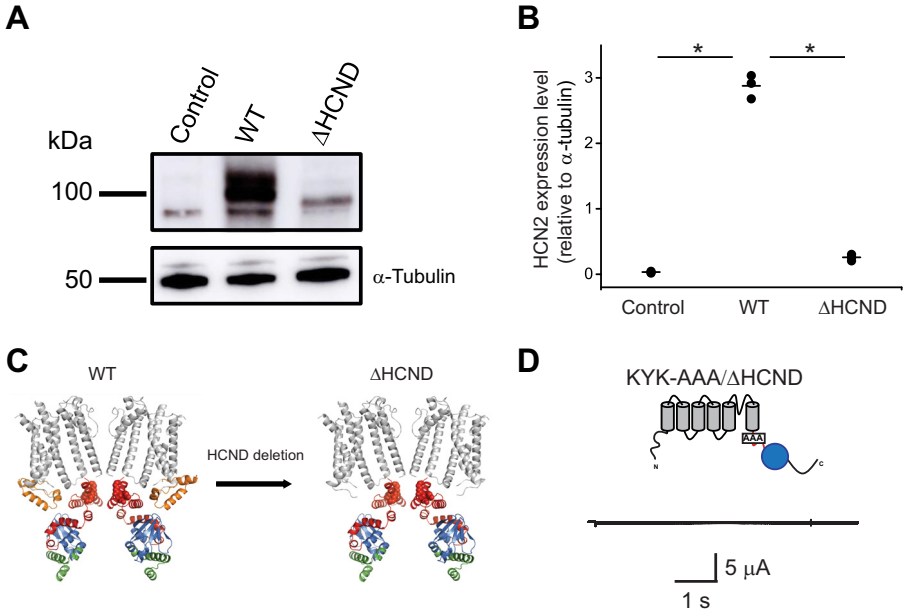

Figure 2. HCND is essential for the surface expression of HCN2 channels. *A*, *top panel*, representative immunoblot of the biotinylated protein fraction for untransfected (control), WT, and ΔHCND mHCN2 transfected HEK293 cells probed with HCN2 specific antibody. *Bottom panel*, representative immunoblot of the whole-cell lysates from untransfected (control), WT, and ΔHCND mHCN2 transfected HEK293 cells probed with α-tubulin antibodies. *B*, quantification of unglycosylated channel expression in untransfected (control), WT, and ΔHCND mHCN2 transfected HEK293 cells. The means of the data are presented as *black lines*. $n = 3$. The data were compared using unpaired Student's *t* test. *, $p < 0.0001$. *C*, ribbon representation of the WT and ΔHCND mutant mHCN2 channels. The same color coding as in Fig. 1*A*, with the KYK ER retention signal residues shown in *red spheres*. *D*, representative currents from KYK_AAA/ΔHCND mutant channels.

nylated, purified from cellular lysates using neutravidin beads, and then visualized using Western blotting. Although HEK293 cells transfected with WT HCN2 channels showed a robust surface expression of *N*-glycosylated and unglycosylated (expected molecular mass, ~100 kDa) channels, as reported previously (24, 25), cells transfected with the ΔHCND mutant channels only expressed unglycosylated channels at substantially lower levels than for WT HCN2 (Fig. 2*A*). No HCN2 channel surface expression was detected for the untransfected HEK293 cells. Staining with the α-tubulin antibody indicated that the levels of loaded protein were similar for all biotinylation experiments (Fig. 2*A*). Similar results were observed in *n* of 3 experiments, as quantified in Fig. 2*B*.

Neutralization of the KYK retention signal fails to rescue currents from ΔHCND channels

To investigate whether the deletion of the HCND exposed an endoplasmic reticulum (ER) retention signal, we searched for subcellular localization signals in the amino acid sequence of HCN2 channels using LocSigDB, a publicly available database of experimental localization signals (26). The search identified a KYK ER retention signal (27, 28). The KYK ER retention signal (residues 452–454 in the mouse HCN2 channels) is located in the C-linker (Fig. 2*C*, *left panel*) and is conserved in all four HCN channel isoforms. Deletion of the HCND would increase the accessibility of the KYK residues (Fig. 2*C*, *right panel*). To test whether neutralizing the KYK ER retention signal could rescue the currents from the ΔHCND mutant mHCN2 channels, we generated mutant mHCN2 channels with alanines substituted for the KYK residues in the background of the HCND deletion (KYK-AAA/ΔHCND). Unfortunately, no hyperpolarization-activated currents were detected for the mutant channels (Fig. 2*D*). Therefore, neutralizing the KYK retention signal failed to rescue loss of HCN2 currents caused by the HCND deletion.

Disrupting interactions between the S2 of the VSD and HCND abolishes currents from HCN2 channels

In addition to the importance for the targeting of HCN channels to the surface, the HCND could also contribute to the gating of HCN channels. To test the functional importance of HCND, we analyzed the contacts it forms with the VSD. Analysis of the HCN1 cryo-EM structure revealed that residues Arg^{195} and Gly^{197} (Arg^{237} and Gly^{239} in HCN2) on the S2 of the VSD directly interact with the residue Ile^{135} (Ile^{177} in HCN2) on the HCND (Fig. 3*A*). To determine the importance of this interaction for the HCN2 channel function, we mutated Arg^{237} and Gly^{239} to alanines. To our surprise, expression of G239A/R237A mutant channels in oocytes did not generate any hyperpolarization-activated currents (Fig. 3*B*). The absence of hyperpolarization-activated currents was observed in $n \geq 60$ independent experiments, performed on oocytes from different batches.

Although we disrupted interactions between the HCND and the S2 of the VSD by mutating Arg^{237} and Gly^{239} residues in the VSD, Porro *et al.* (22) considered mutations of the Ile^{177} residue on the HCND. Although mutating Ile^{177} to a valine or alanine generated currents similar to the ones from WT HCN2 channels, substituting an aspartic acid or glycine for Ile^{177} abolished HCN2 channel currents. Moreover, confocal microscopy analysis indicated the absence of expression of the I177D and I177G mutant channels at the membrane surface. In agreement with our findings, these results could underscore the importance of

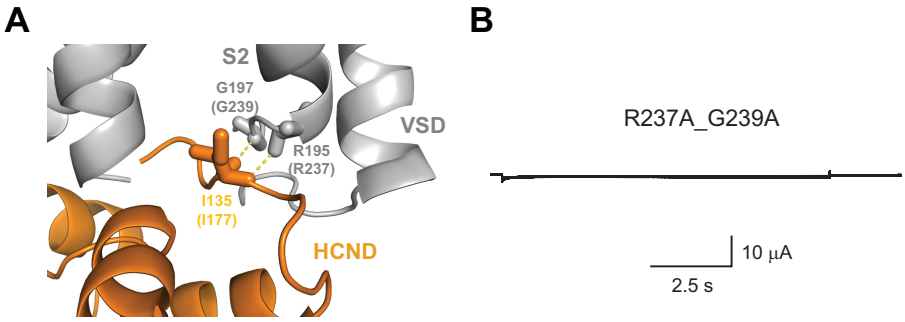

Figure 3. Interactions between the HCND and S2 are required for the HCN2 channel function. *A*, enlarged view of the interaction interface between the HCND and the VSD in HCN1 channel structure. The interacting residues Gly[197] and Arg[195] on the S2 and Ile[135] on the HCND are shown as *sticks*. Corresponding residues in HCN2 channels are shown in *parentheses*. *B*, representative currents from R237A/G239A mutant mHCN2 channels.

the VSD/HCND interactions for the functional expression of HCN2 channels.

Disrupting interactions between the CNBD and HCND affects both voltage- and cAMP-dependent gating of HCN2 channels

In the HCN1 channel cryo-EM structure, in addition to interacting with the VSD, the HCND also interacts with the CNBD. The structural analysis indicted that residues Glu[436] and Gln[440] (Glu[478] and Gln[482] in HCN2) on the C-linker directly interact with the residue Arg[112] (Arg[154] in HCN2) of the HCND of the adjacent subunit, and His[517] (His[559] in HCN2) in the CNBD directly interacts with the residue Ser[116] (Ser[158] in HCN2) in the HCND of the adjacent subunit (Fig. 4*A*). If the HCND forms a functional link between the VSD and CNBD then disrupting these interactions should change both the voltage-dependent and cyclic nucleotide– dependent gating of the channels. To test this hypothesis, we generated a triple mutant HCN2 channels (3M: E478A/Q482A/H559A) with the three residues on the C-linker–CNBD that interact with the HCND mutated to alanines. The 3M mutant channels gave rise to the hyperpolarization-activated currents (Fig. 4*B*). Analysis of the conductance *versus* voltage relationship indicated that the average $V_{½}$ was -91.3 ± 0.3 ($n = 9$) for WT channels and -97.1 ± 0.3 mV ($n = 10$) for the 3M mutant channels (Fig. 4*C*). Therefore, disrupting the interactions between the CNBD and HCND shifted the voltage dependence of the channel activation to more hyperpolarized voltages by ~6 mV. This is a small but statistically significant shift ($p = 0.0001$ by the unpaired Student's *t* test). The shift in the voltage dependence suggests that the HCND functionally couples the CNBD and VSD in HCN2 channels.

To test whether disrupting the interactions between the HCND and C-linker–CNBD also affects cyclic nucleotide– dependent activation of HCN2 channels, we examined currents from WT and 3M channels over a range of cAMP concentrations. These experiments were performed using excised inside-out patch-clamp configuration, where cAMP, at the indicated concentrations, was directly applied to the intracellular side of HCN2 channels containing the CNBDs. Application of 10 μM cAMP increased the steady-state and tail currents for both WT (Fig. 5*A*) and 3M mutant channels (Fig. 5*B*). The average increase was 58 ± 12% for WT channels and 86 ± 15% for 3M mutant channels in the presence of 10 μM cAMP (Fig. 5*C*). The increase in the cAMP-dependent current facilitation was greater for the 3M channels for all tested cAMP concentrations (Fig. 5*C*). The difference was statistically significant ($p < 0.001$ by two-way analysis of variance), suggesting that the magnitude of the cAMP effect (potency) is increased in 3M mutant channels. The apparent cAMP affinity was 100 ± 40 nM for WT and 60 ± 20 nM for 3M mutant channels. The difference in the affinities was not statistically significant, as calculated by unpaired Student's *t* test.

We also analyzed the effect of the 3M mutation on the kinetics of the HCN current activation and deactivation in the absence and presence of 10 μM cAMP. The time constants of activation and deactivation were determined by fitting the activation currents and tail currents, correspondingly, with a single exponential function. Although the average time constants of activation were statistically similar for WT and 3M mutant channels, in both the absence and the presence of cAMP, the time constant of deactivation was larger for 3M mutant channels (Fig. 5*D*). This indicates that the 3M mutation slows down deactivation in the absence of cAMP. Interestingly, if for WT channels the deactivation was slower in the presence of cAMP, for 3M mutant channels cAMP accelerated the deactivation. These findings indicate that disrupting interactions between the HCND and C-linker–CNBD alters the energetics of CNBD interaction with the rest of the channel and, therefore, affects not only the voltage-dependent (Fig. 4*C*) but also cyclic nucleotide– dependent gating. Porro *et al.* (22) also found that disrupting the interactions between the HCND and C-linker–CNBD alters both voltage and cAMP sensitivity of HCN channels, although their conclusion is based on examining mostly different interacting residues, as discussed below.

Discussion

In this study we investigated the functional importance of the HCND and direct contacts it forms with the VSD and CNBD for HCN2 channel gating. Deletion of the HCND inhibited surface expression of HCN2 channels and disruption of the contacts between the HCND and VSD abolished currents from HCN2 channels. Therefore, the HCND is required for the expression of functional HCN channels. Disruption of the direct contacts between the HCND and C-linker–CNBD affected both voltage- and cyclic nucleotide– dependent gating of HCN channels, suggesting that the HCND provides not only structural but also functional link between the voltage- and cyclic nucleotide–sensing mechanisms in HCN channels.

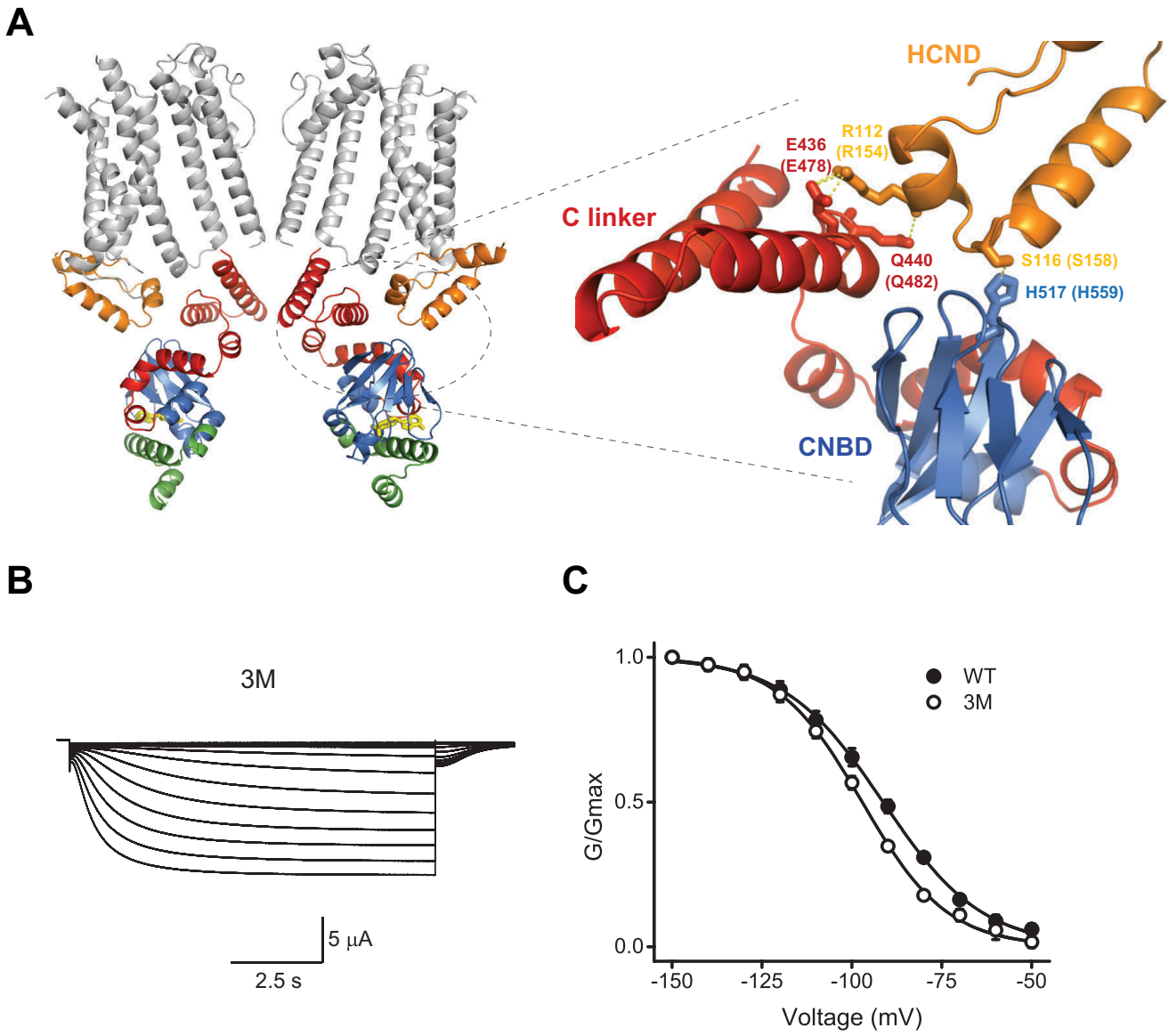

Figure 4. Interactions between the HCND and C-linker–CNBD affect voltage-dependent gating of HCN2 channels. *A*, enlarged view of the interaction interface between the HCND and the C-linker–CNBD in HCN1 channels. The interacting residues Glu^{436} and Gln^{440} on the C-linker, His^{517} on the CNBD, and Arg^{112} on the HCND are shown as *sticks*. Corresponding residues in HCN2 channels are shown in *parentheses*. *B*, representative currents from E478A/Q482A/H559A (3M) mutant mHCN2 channels. *C*, averaged conductance–voltage relationship for the currents from WT (*filled circles*, *n* of 9) and 3M mutant (*open circles*, n of 10) mHCN2 channels. *Lines* correspond to the fits with the Boltzmann function with the $V_{1/2}$ of −91.3 ± 0.3 mV for WT and −97.1 ± 0.3 mV for the 3M mutant, and *s* of 13.8 ± 0.2 for WT and 11.9 ± 0.3 for 3M mutant mHCN2 channels.

Previous studies have shown that the N terminus is essential for the surface expression of HCN channels. Deletion of the entire N terminus (residues 1–185) abolished currents from HCN2 channels and prevented their surface expression, as indicated by the confocal images of the WT and N-terminal deleted HCN2 channels fused with GFP (29). Similarly, HCN1 channels lacking the N terminus were retained in the ER (30). Our results show that even if the first 136 N-terminal residues are intact but 45 residues forming the HCND (residues 137–180) are missing, expression of HCN2 channels at the surface is drastically decreased, and currents are abolished (Figs. 1*D* and 2). Interestingly, the mutant ΔHCND HCN2 channels were still detected at the surface but at levels substantially lower than the WT channels. Although for the WT channels Western blotting analysis showed both glycosylated and nonglycosylated populations at the surface, for ΔHCND channels no glycosylated population was detected under the examined experimental conditions. It has been shown that the *N*-glycosylation is present in native HCN channels in the brain and recombinant HCN channels expressed in HEK293 cells (25). Inhibiting *N*-linked glycosylation with tunicamycin and mutating the putative glycosylation site (Asn^{380}) abolished currents and prevented surface expression of HCN2 channels in HEK293 cells (25). In our experiments, the absence of the glycosylated ΔHCND mutant channel at the surface suggests that the deletion of the HCND prevents N-terminal glycosylation most likely by interfering with the proper folding of the protein.

Our study indicates that, in addition to affecting the surface expression, the HCND is also an important functional element

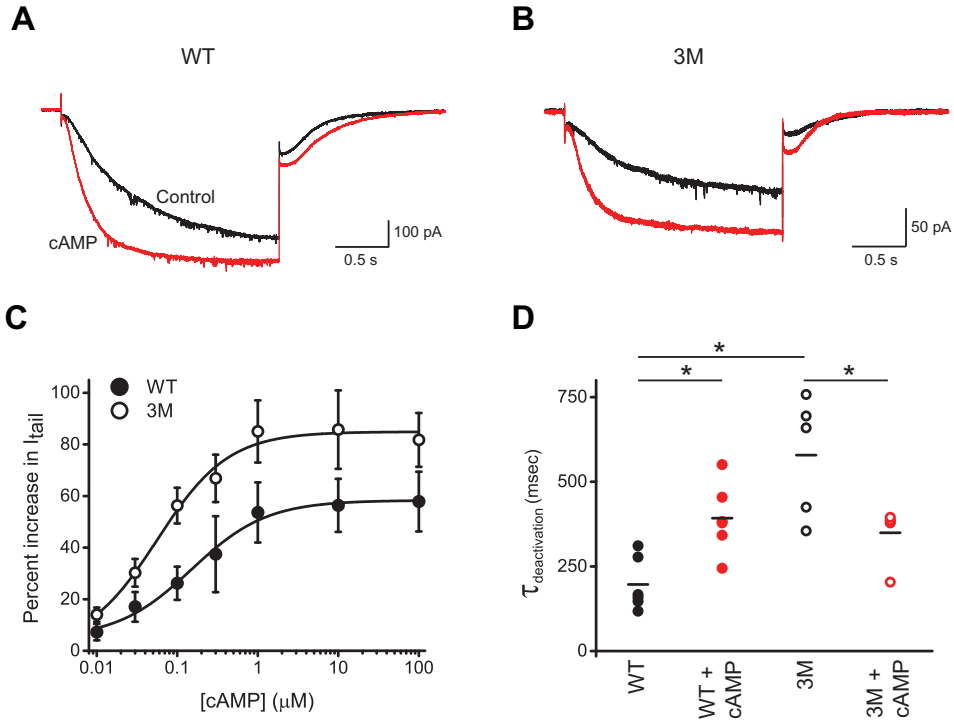

Figure 5. Interactions between the HCND and C-linker–CNBD affect the cAMP-dependent gating of HCN2 channels. *A* and *B*, representative currents from WT (*A*) and 3M mutant (*B*) mHCN2 channels recorded at −90 mV in the absence (*black*) and presence (*red*) of 10 μM cAMP. *C*, plots of the percentage of increase in tail currents *versus* the cAMP concentration for WT (*filled circles*) and 3M (*open circles*) mutant mHCN2 channels. The tail currents were recorded at −40 mV after the test pulse to −90 mV. *Lines* correspond to the fits with the Hill equation with the K_d of 100 ± 40 nM for WT and 60 ± 20 nM for 3M mutant mHCN2 channels. $n \geq 5$ for each condition. *D*, plots of deactivation time constants for tail currents recorded at −40 mV after the test pulse to −90 mV for WT and 3M mutant channels in the presence and absence of 10 μM cAMP, as indicated. The means of the data are presented as *black lines*. $n = 6$ for WT and $n = 5$ for 3M mutant channels. The data with and without cAMP for WT and 3M channels were compared using paired Student's *t* test. The data between WT and 3M mutant channels were compared using unpaired Student's *t* test. * $p < 0.02$.

for fine-tuning both cNMP and voltage-dependent gating of HCN channels. HCN channel opening requires membrane hyperpolarization (1, 2). Although the dislocation of the VSD is substantial, as deduced based on the changes in the transition metal ion FRET with membrane hyperpolarization (31) and structural analysis of the cross-linked HCN1 channels with the VSD in a hyperpolarized state (32), the movement of the VSD in response to the hyperpolarization that results in the channel opening is not clear. The VSD is connected to the PD via the S4-S5 linker (17). Mutations in the S4-S5 linker affect the voltage-dependent gating of HCN channels (33). However, the S4-S5 linker is not required for the HCN channel opening with hyperpolarization because co-expression of the VSD and PD of spHCN (sea urchin HCN) channels as separate proteins generated hyperpolarization-activated currents (34). It has been proposed that an extensive interface between the S4 and S5 in HCN channels is responsible for the apparent hyperpolarization-dependent activation in HCN channels (35). Consistent with this hypothesis, co-expression of the PD with the VSD lacking the C-terminal end of the S4 resulted in cNMP-modulated but voltage-independent channels (34) and cross-linking the S4 and S5 could lock the channels in the "locked-open" or "locked-closed" states (36, 37). More recent structural analysis of the cross-linked HCN1 channels and molecular dynamics simulations indicated that during the hyperpolarization-dependent gating, the S4 helix breaks into two helices (32, 38). Because the HCND forms direct interactions with the VSD, it could also contribute to the VSD movement during the voltage-dependent gating. Surprisingly, disrupting the VSD and HCND interactions with a double mutation R237A/G239A in the S2 of the VSD resulted in nonfunctional channels (Fig. 3*B*). The reason for such a dramatic effect is not clear. Possible explanations could be that the S2–HCND interactions are crucial for the function of HCN channels and/or that the Arg^{237} and Gly^{239} residues are important for the folding of the channel.

It is thought that in the absence of cyclic nucleotides, the intracellular C-linker–CNBD inhibits HCN channel opening, and binding of cyclic nucleotides removes this autoinhibition (1, 2). The interface between the intracellular C-linker–CNBDs from different subunits is formed by the "elbow-on-shoulder" interactions, in which the elbow formed by A′–B′ α helices of the C-linker of one subunit is resting on the shoulder formed by the C′–D′ α helices of the C-linker of an adjacent subunit (18, 39). In this manner, the C-linkers bring together the CNBDs in a tetrameric ring that undergoes conformational changes upon cyclic nucleotide binding, facilitating the channel opening (39–41). The HCN1 channel structure revealed that in addition to the elbow-on-shoulder interactions, the C-linker–CNBDs also form intersubunit interactions with the HCNDs (Fig. 4*A*). Therefore, cNMP-dependent gating of HCN channels most likely is accompanied not just by the rearrangement of the elbow-on-shoulder interface but also of the interface between the HCND and C-linker–CNBD. Our results show that breaking the intersubunit interactions between the HCND and C-linker–CNBD affects the CNBD-dependent gating of HCN2 channels by increasing the potency of HCN current facilitation

by cAMP, slowing down the current deactivation in the absence of cAMP and accelerating the deactivation in the presence of cAMP (Fig. 5, *C* and *D*). This suggests that the intersubunit interactions between the HCND and C-linker–CNBDs change the energetics of channel gating by the CNBD.

Another important conclusion of the HCN1 structure is that the HCND provides a direct structural link between the VSD and C-linker–CNBD. Here we tested the functional significance of this structural link. In addition to the effect on the cAMP-dependent gating, as discussed above, disrupting the interactions between the HCND and C-linker–CNBD shifted the conductance *versus* voltage plots to more hyperpolarized potentials (Fig. 4*C*). These findings suggest that the HCND provides a direct functional link between the voltage- and cNMP-dependent gating mechanisms and decreases the energetic barrier for channel activation with hyperpolarization. Consistent with our finding, Yellen and co-workers (36) have shown that cross-linking the C-linker with the S4 in the VSD could result in a locked-open or lock-closed channels.

During the final stages of our study, Porro *et al.* (22) published a study on the role of the HCND in HCN channel gating. They also concluded that the HCND couples the voltage and cAMP sensing in HCN channels and that the interactions between the HCND and VSD are crucial for surface expression of the channels. Although the main findings of Porro *et al.* (22) are similar to ours, the two studies differ substantially in the approaches used. In our study we used surface biotinylation assay to show that deletion of the HCND prevents HCN2 channel expression at the membrane surface of *Xenopus* oocytes. Porro *et al.* (22) used confocal microscopy analysis to show that mutant HCN2 and HCN1 channels with disturbed interactions between the HCND and VSD are not targeted to the plasma membrane of HEK293T cells.

While we focused on disrupting the interactions between the VSD and Ile^{177} in the HCND by introducing mutations in the interacting residues Arg^{237} and Gly^{239} on the VSD, Porro *et al.* (22) primarily introduced mutations in the Ile^{177} and adjacent residues on the HCND. Both approaches would disrupt interactions between the HCND and VSD. However, because the HCND forms interactions with both C-linker–CNBD and VSD, to make sure that disrupting interactions between the HCND and VSD does not affect the pathways dependent on the HCND and C-linker–CNBD interactions, introducing mutations in the residues on the VSD would be advantageous. In agreement with our findings, the analysis by Porro *et al.* (22) demonstrated that interactions between the Ile^{177}/Ile^{135} residue and the VSD in HCN2/HCN1 channels is crucial for HCN channel function because I177D and I177G mutant HCN2 channels, and I135G mutant HCN1 channels did not generate any detectable currents. Porro *et al.* (22) also considered L250A mutation on the S2-S3 loop of the VSD, which decreased the channel expression and drastically changed the kinetics of channel activation. However, Leu^{250} does not make direct interactions with Ile^{177}, and therefore, it is difficult to compare the observed effect with what we are reporting here. In addition, Porro *et al.* (22) reported that another residue on the HCND, Phe^{109} (Phe^{151} in HCN2), forms direct interactions with the S1 and S4 of the VSD. Disruption of these interactions drastically affected the voltage-dependent gating of HCN2 and HCN1 channels. Therefore, experiments in both studies show that disrupting contacts between the HCND and VSD affects the voltage-dependent gating of HCN channels.

Both studies investigated the contacts formed between the HCND and C-linker–CNBD and identified Arg^{112} (Arg^{154} in HCN2) as one of the residues on the HCND forming direct interactions with the C-linker–CNBD. However, although1 we determined that Arg^{112} interacts with Glu^{436} and Gln^{440} (Glu^{478} and Gln^{482} in HCN2) on the C-linker, Porro *et al.* (22) determined that the only residue on the C-linker interacting with Arg^{112} is Glu^{436}. Also, although we determined that another pair of interacting residues between the HCND and C-linker–CNBD is Ser^{116}–His^{517} (Ser^{158}–His^{559} in HCN2), Porro *et al.* (22) identified Met^{113}–Lys^{422} (Met^{155}–Lys^{464} in HCN2). To disrupt the interactions between the HCND and C-linker–CNBD, we introduced a triple mutation in HCN2 channels with alanines substituted for Glu^{478}, Gln^{482}, and His^{559} residues. We show that the triple mutant channel had altered voltage and cAMP sensitivity. Based on their structural analysis, to disrupt the interactions between the HCND and C-linker–CNBD, Porro *et al.* (22) considered individual and double mutations of Lys^{464} and Glu^{478} residues to alanines. The individual K464A and E478A mutations had opposite effects on the voltage dependence of HCN2 channels, with the former shifting the conductance *versus* voltage dependence of HCN2 channels to the depolarized potentials and the latter to the hyperpolarized potentials. The double mutant K464A/E478A had similar voltage dependence to the WT HCN2 channels. Importantly, when introduced individually, K464A and E478A mutations had no effect on the cAMP sensitivity, however, the double K464A/E478A mutant channel activation was insensitive to cAMP, with only the deactivation kinetics affected by cAMP (22). Therefore, similar to the results for the triple-mutant channel in our study, in the study by Porro *et al.* (22), disrupting the interactions between the HCND and C-linker–CNBD affected both voltage and cAMP sensitivity of HCN channels. Taking together the effect of all examined mutations, both we and Porro *et al.* (22) concluded that the HCND provides a functional link between the voltage- and cNMP-dependent gating mechanisms in HCN channels. It is reassuring that examination of distinct interactions by the two studies led to similar conclusions, which provides complementary evidence for the critical role of the HCND in HCN channel surface expression and functional coupling of its voltage- and cAMP-dependent gating mechanisms

Recently, it has been proposed that the voltage-dependent gating of HCN and related depolarization-activated KCNH channels is more conserved than previously thought (35). The VSD of HCN channels is capable of activating the channels with depolarization, but this ability is masked by rapid inactivation. The HCND is conserved in HCN channels and is missing in KCNH channels. Therefore, although the other voltage-dependent mechanisms could be similar between the HCN and KCNH channel families, the HCND seems to provide unique means to fine-tune the voltage and cNMP dependence in HCN channels.

Experimental procedures

Electrophysiology

The cDNA encoding mouse HCN2 channels in pGEMHE vector was kindly provided by Steven Siegelbaum (Columbia University, New York, NY). Mutant HCN2 channels used in the study were generated by Bio Basic Inc. and subcloned into pGEMHE vector. The amino acid sequence of the mutant channels was confirmed using DNA sequencing (Genewiz). The cRNA was transcribed using the T7 mMessage mMachine kits (Thermo Fisher Scientific). Defolliculated *X. laevis* oocytes were purchased from Ecocyte Bioscience (Austin, TX), injected with the cRNA using a Nanoinject II oocyte injector (Drummond), and incubated at 18 °C. HCN2 currents were recorded at room temperature with either TEVC amplifier (OC-725C, Warner Instruments) or with Axopatch 200A patch-clamp amplifier (Molecular Devices) for excised inside-out membrane patches. The signals were digitized using Digidata 1550 and pClamp11 software (Molecular Devices).

For TEVC experiments, oocytes were placed into a RC-3Z chamber (Warner Instruments). Glass pipettes were pulled from borosilicate glass and had resistances of 0.8–1.5 MΩ when filled with 3 M KCl. The recording (bath) solution contained 100 mM KCl, 10 mM HEPES, 1 mM EGTA, pH 7.3. HCN currents were elicited by applying a series of 5-s voltage pulses (ranging from −150 to −40 mV in 10-mV increments) from a holding potential of 0 mV, followed by a 1-s voltage tail pulse to −40 mV. The currents were not leak-subtracted. For currents recorded from excised membrane patches, the oocytes, following a manual removal of the vitelline membrane, were transferred to a handmade chamber containing the bath solution. Patch pipettes were pulled from borosilicate glass and had a resistance of 0.5–1.2 MΩ after fire polishing. The extracellular (pipette) solutions contained 130 mM KCl, 10 mM HEPES, 0.2 mM EDTA, pH 7.2. The intracellular (bath) solution was either the same as the pipette solution or contained cAMP at the indicated concentrations. HCN currents were elicited by applying 5-s voltage pulses at −90 mV from a holding potential of 0 mV, followed by a 1-s voltage tail pulse to −40 mV.

To analyze voltage dependence of HCN channel activation, peak tail-current amplitudes were normalized to the largest peak tail-current amplitude (G_{max}). The normalized amplitudes were then plotted against the test voltage and fitted with a Boltzmann equation,

$$\frac{G}{G_{max}} = \frac{1}{1 + e\left(\frac{V - V_{1/2}}{s}\right)} \quad \text{(Eq. 1)}$$

where V represents the test voltage (mV), $V_{½}$ is the midpoint activation voltage (mV), and s is the slope of the relation (mV).

cAMP was purchased from Sigma. cAMP stock was prepared in the bath solution and then diluted to obtain the range of concentrations used for the dose-response experiments. The bath solution was changed using a gravity-fed solution changer. To determine the apparent cAMP affinity (K_d), the percentage of increase in the peak tail current recorded after the test pulse to −90 mV was plotted *versus* the concentration of cAMP and fitted with a Hill equation,

$$Y[X] = Y_0 + \left(\frac{(Y_\infty + Y_0)}{\left(1 + \left(\frac{K_d}{x}\right)^n\right)}\right) \quad \text{(Eq. 2)}$$

where Y_0 represents the minimum % increase, Y_∞ is the maximum, and n is the Hill coefficient.

The data analysis and fitting of the plots were performed in Clampfit (Molecular Devices) and Origin (Microcal Software, Inc.). The *error bars* in the figures correspond to the S.E. Statistical analysis was performed using paired or unpaired Student's t tests and two-way analysis of variance, as indicated. p values < 0.05 were considered significant. n represents the number of recordings from different oocytes (for TEVC experiments) or patches (for current recordings from inside-out membrane patches).

Channel expression in HEK293 cells

For the surface biotinylation experiments, mHCN2 channels were transfected into HEK293 cells. The cDNA encoding mHCN2 channels in pcDNA3 vector for mammalian expression was kindly provided by Juliane Stieber and Andreas Ludwig (Institute for Pharmacology, Friedrich-Alexander-University, Erlangen-Nuremberg, Germany). The mutant cDNA with the deletion of the HCND was synthesized by Bio Basic Inc. and subcloned into pcDNA3 vector. The amino acid sequence of the synthesized gene was confirmed using DNA sequencing (Genewiz).

HEK293 cells were cultured and transfected with the WT and mutant mHCN2 channels as described (42). 24 h prior to transfection, the cells were plated at a cell density of $1–3 \times 10^5$ cells into 60-mm dishes. The transfection was performed using the TransIT-LT1 transfection reagent (Mirus) according to the manufacturer's protocol.

Biotinylation assay

All biotinylation steps were performed at 4 °C. At 48 h post-transfection, HEK293 cells were washed twice with ice-cold PBS and incubated in PBS with 1 mg/ml EZ-Link Sulfo-NHS-SS-Biotin (Thermo Fisher Scientific, PI21331) for 30 min. The biotin-containing solution was then removed, and unreacted biotin was quenched by washing the cells with 50 mM Tris-Cl, pH 7.5, for 20 min. The cells were then washed three times with ice-cold PBS and lysed with the buffer containing 1% Triton X-100, 150 mM NaCl, 20 mM EDTA, 10 mM EGTA, 25 mM Tris-Cl, pH 7.4, and 5 mg/ml of leupeptin, antipain, and pepstatin. The lysates were centrifuged for 15 min at 15,000 × *g*, and supernatants were transferred to clean 1.5-ml microcentrifuge tubes containing immobilized neutravidin beads (Thermo Fisher Scientific, PI29200) washed with ice-cold PBS. After 2 h of incubation with a rotator, the tubes were centrifuged for 5 min at 2,000 × *g*. The beads were washed five times with PBS supplemented with 0.1% SDS and centrifuged between washes.

SDS-PAGE and Western blotting

The biotinylated proteins were eluted off the beads by adding 2× Laemmli sample buffer at 95 °C for 5 min and loaded on 12%

Bis-Tris SDS-polyacrylamide gels. After SDS-PAGE, the proteins were transferred to a nitrocellulose membrane by electroblotting. The HCN channels were detected using a rabbit anti-HCN2 primary antibody (Boster, A02804) that recognizes the C-terminal sequence of HCN2 channels and a goat anti-rabbit secondary antibody (Abcam, ab6721). Chemiluminescent signal was detected using SuperSignal West Femto maximum sensitivity substrate chemiluminescence detection kit (Pierce). As a loading control, we used α-tubulin antibody (Thermo Fisher Scientific, NB100690SS). The band intensities were analyzed with ImageJ.

Data availability

All data are contained within the manuscript.

Acknowledgments—We are grateful to William N. Zagotta for helpful discussions. We thank Gerard Ahern for generously allowing us to use his lab equipment to carry out the initial experiments for the project and to Robert Yasuda for providing the HEK293 cell cultures for our experiments.

Author contributions—Z.-J. W., I. B., and S. H. data curation; Z.-J. W., I. B., S. H., and T. I. B. formal analysis; Z.-J. W., I. B., S. H., and T. I. B. validation; Z.-J. W., I. B., S. H., and T. I. B. investigation; Z.-J. W., I. B., S. H., and T. I. B. visualization; Z.-J. W., I. B., and T. I. B. methodology; Z.-J. W., I. B., S. H., and T. I. B. writing-review and editing; I. B. and T. I. B. resources; T. I. B. conceptualization; T. I. B. supervision; T. I. B. funding acquisition; T. I. B. writing-original draft; T. I. B. project administration.

Funding and additional information—This work was supported by NIGMS, National Institutes of Health Grant R01GM124020 (to T. I. B.). The content is solely the responsibility of the authors and does not necessarily represent the official views of the National Institutes of Health.

Conflict of interest—The authors declare that they have no conflicts of interest with the contents of this article.

Abbreviations—The abbreviations used are: HCN, hyperpolarization-activated cyclic nucleotide-gated; HCND, HCN domain; cNMP, cyclic nucleotide; VSD, voltage sensor domain; CNBD, cyclic nucleotide-binding domain; PD, pore domain; TEVC, two-electrode voltage-clamp; ER, endoplasmic reticulum.

References

1. Ludwig, A., Zong, X., Jeglitsch, M., Hofmann, F., and Biel, M. (1998) A family of hyperpolarization-activated mammalian cation channels. *Nature* **393,** 587–591 CrossRef Medline
2. Santoro, B., Liu, D. T., Yao, H., Bartsch, D., Kandel, E. R., Siegelbaum, S. A., and Tibbs, G. R. (1998) Identification of a gene encoding a hyperpolarization-activated pacemaker channel of brain. *Cell* **93,** 717–729 CrossRef Medline
3. DiFrancesco, D., and Tortora, P. (1991) Direct activation of cardiac pacemaker channels by intracellular cyclic AMP. *Nature* **351,** 145–147 CrossRef Medline
4. Wahl-Schott, C., and Biel, M. (2009) HCN channels: structure, cellular regulation and physiological function. *Cell Mol. Life Sci.* **66,** 470–494 CrossRef Medline
5. Kaupp, U. B., and Seifert, R. (2001) Molecular diversity of pacemaker ion channels. *Annu. Rev. Physiol.* **63,** 235–257 CrossRef Medline
6. DiFrancesco, D. (2010) The role of the funny current in pacemaker activity. *Circ. Res.* **106,** 434–446 CrossRef Medline
7. Santoro, B., Chen, S., Luthi, A., Pavlidis, P., Shumyatsky, G. P., Tibbs, G. R., and Siegelbaum, S. A. (2000) Molecular and functional heterogeneity of hyperpolarization-activated pacemaker channels in the mouse CNS. *J. Neurosci.* **20,** 5264–5275 CrossRef Medline
8. Dibbens, L. M., Reid, C. A., Hodgson, B., Thomas, E. A., Phillips, A. M., Gazina, E., Cromer, B. A., Clarke, A. L., Baram, T. Z., Scheffer, I. E., Berkovic, S. F., and Petrou, S. (2010) Augmented currents of an HCN2 variant in patients with febrile seizure syndromes. *Ann. Neurol.* **67,** 542–546 CrossRef Medline
9. Tang, B., Sander, T., Craven, K. B., Hempelmann, A., and Escayg, A. (2008) Mutation analysis of the hyperpolarization-activated cyclic nucleotide-gated channels HCN1 and HCN2 in idiopathic generalized epilepsy. *Neurobiol. Dis.* **29,** 59–70 CrossRef Medline
10. DiFrancesco, J. C., Barbuti, A., Milanesi, R., Coco, S., Bucchi, A., Bottelli, G., Ferrarese, C., Franceschetti, S., Terragni, B., Baruscotti, M., and DiFrancesco, D. (2011) Recessive loss-of-function mutation in the pacemaker HCN2 channel causing increased neuronal excitability in a patient with idiopathic generalized epilepsy. *J. Neurosci.* **31,** 17327–17337 CrossRef Medline
11. Nakamura, Y., Shi, X., Numata, T., Mori, Y., Inoue, R., Lossin, C., Baram, T. Z., and Hirose, S. (2013) Novel HCN2 mutation contributes to febrile seizures by shifting the channel's kinetics in a temperature-dependent manner. *PLoS One* **8,** e80376 CrossRef Medline
12. Nava, C., Dalle, C., Rastetter, A., Striano, P., de Kovel, C. G., Nabbout, R., Cancès, C., Ville, D., Brilstra, E. H., Gobbi, G., Raffo, E., Bouteiller, D., Marie, Y., Trouillard, O., Robbiano, A., *et al.* (2014) *De novo* mutations in HCN1 cause early infantile epileptic encephalopathy. *Nat. Genet.* **46,** 640–645 CrossRef Medline
13. DiFrancesco, D. (1993) Pacemaker mechanisms in cardiac tissue. *Annu. Rev. Physiol.* **55,** 455–472 CrossRef Medline
14. Shi, W., Wymore, R., Yu, H., Wu, J., Wymore, R. T., Pan, Z., Robinson, R. B., Dixon, J. E., McKinnon, D., and Cohen, I. S. (1999) Distribution and prevalence of hyperpolarization-activated cation channel (HCN) mRNA expression in cardiac tissues. *Circ. Res.* **85,** e1–e6 Medline
15. Möller, M., Silbernagel, N., Wrobel, E., Stallmayer, B., Amedonu, E., Rinné, S., Peischard, S., Meuth, S. G., Wünsch, B., Strutz-Seebohm, N., Decher, N., Schulze-Bahr, E., and Seebohm, G. (2018) *In vitro* analyses of novel HCN4 gene mutations. *Cell Physiol. Biochem.* **49,** 1197–1207 CrossRef Medline
16. Schulze-Bahr, E., Neu, A., Friederich, P., Kaupp, U. B., Breithardt, G., Pongs, O., and Isbrandt, D. (2003) Pacemaker channel dysfunction in a patient with sinus node disease. *J. Clin. Invest.* **111,** 1537–1545 CrossRef Medline
17. Lee, C. H., and MacKinnon, R. (2017) Structures of the human HCN1 hyperpolarization-activated channel. *Cell* **168,** 111–120.e11 CrossRef Medline
18. Zagotta, W. N., Olivier, N. B., Black, K. D., Young, E. C., Olson, R., and Gouaux, E. (2003) Structural basis for modulation and agonist specificity of HCN pacemaker channels. *Nature* **425,** 200–205 CrossRef Medline
19. Wicks, N. L., Chan, K. S., Madden, Z., Santoro, B., and Young, E. C. (2009) Sensitivity of HCN channel deactivation to cAMP is amplified by an S4 mutation combined with activation mode shift. *Pflugers Arch.* **458,** 877–889 CrossRef Medline
20. Kusch, J., Biskup, C., Thon, S., Schulz, E., Nache, V., Zimmer, T., Schwede, F., and Benndorf, K. (2010) Interdependence of receptor activation and ligand binding in HCN2 pacemaker channels. *Neuron* **67,** 75–85 CrossRef Medline
21. Hummert, S., Thon, S., Eick, T., Schmauder, R., Schulz, E., and Benndorf, K. (2018) Activation gating in HCN2 channels. *PLoS Comput. Biol.* **14,** e1006045 CrossRef Medline
22. Porro, A., Saponaro, A., Gasparri, F., Bauer, D., Gross, C., Pisoni, M., Abbandonato, G., Hamacher, K., Santoro, B., Thiel, G., and Moroni, A. (2019) The HCN domain couples voltage gating and cAMP response in hyperpolarization-activated cyclic nucleotide-gated channels. *Elife* **8,** e49672, CrossRef
23. Wang, Z. J., Hayoz, S., and Brelidze, T. I. (2019) The role of HCN domain in the function of HCN channels. *Biophys. J.* **116,** 103A CrossRef

24. Akhavan, A., Atanasiu, R., Noguchi, T., Han, W., Holder, N., and Shrier, A. (2005) Identification of the cyclic-nucleotide-binding domain as a conserved determinant of ion-channel cell-surface localization. *J. Cell Sci.* **118,** 2803–2812 CrossRef Medline
25. Much, B., Wahl-Schott, C., Zong, X., Schneider, A., Baumann, L., Moosmang, S., Ludwig, A., and Biel, M. (2003) Role of subunit heteromerization and *N*-linked glycosylation in the formation of functional hyperpolarization-activated cyclic nucleotide-gated channels. *J. Biol. Chem.* **278,** 43781–43786 CrossRef Medline
26. King, B. R., and Guda, C. (2007) ngLOC: an n-gram–based Bayesian method for estimating the subcellular proteomes of eukaryotes. *Genome Biol.* **8,** R68 CrossRef Medline
27. Jackson, M. R., Nilsson, T., and Peterson, P. A. (1990) Identification of a consensus motif for retention of transmembrane proteins in the endoplasmic reticulum. *EMBO J.* **9,** 3153–3162 CrossRef Medline
28. Nilsson, T., Jackson, M., and Peterson, P. A. (1989) Short cytoplasmic sequences serve as retention signals for transmembrane proteins in the endoplasmic reticulum. *Cell* **58,** 707–718 CrossRef Medline
29. Proenza, C., Tran, N., Angoli, D., Zahynacz, K., Balcar, P., and Accili, E. A. (2002) Different roles for the cyclic nucleotide binding domain and amino terminus in assembly and expression of hyperpolarization-activated, cyclic nucleotide-gated channels. *J. Biol. Chem.* **277,** 29634–29642 CrossRef Medline
30. Pan, Y., Laird, J. G., Yamaguchi, D. M., and Baker, S. A. (2015) An N-terminal ER export signal facilitates the plasma membrane targeting of HCN1 channels in photoreceptors. *Invest. Ophthalmol. Vis. Sci.* **56,** 3514–3521 CrossRef Medline
31. Dai, G., Aman, T. K., DiMaio, F., and Zagotta, W. N. (2019) The HCN channel voltage sensor undergoes a large downward motion during hyperpolarization. *Nat. Struct. Mol. Biol.* **26,** 686–694 CrossRef Medline
32. Lee, C. H., and MacKinnon, R. (2019) Voltage sensor movements during hyperpolarization in the HCN channel. *Cell* **179,** 1582–1589.e7 CrossRef Medline
33. Chen, J., Mitcheson, J. S., Tristani-Firouzi, M., Lin, M., and Sanguinetti, M. C. (2001) The S4–S5 linker couples voltage sensing and activation of pacemaker channels. *Proc. Natl. Acad. Sci. U.S.A.* **98,** 11277–11282 CrossRef Medline
34. Flynn, G. E., and Zagotta, W. N. (2018) Insights into the molecular mechanism for hyperpolarization-dependent activation of HCN channels. *Proc. Natl. Acad. Sci. U.S.A.* **115,** E8086–E8095 CrossRef Medline
35. Cowgill, J., Klenchin, V. A., Alvarez-Baron, C., Tewari, D., Blair, A., and Chanda, B. (2019) Bipolar switching by HCN voltage sensor underlies hyperpolarization activation. *Proc. Natl. Acad. Sci. U.S.A.* **116,** 670–678 CrossRef Medline
36. Kwan, D. C., Prole, D. L., and Yellen, G. (2012) Structural changes during HCN channel gating defined by high affinity metal bridges. *J. Gen. Physiol.* **140,** 279–291 CrossRef Medline
37. Shin, K. S., Rothberg, B. S., and Yellen, G. (2001) Blocker state dependence and trapping in hyperpolarization-activated cation channels: evidence for an intracellular activation gate. *J. Gen. Physiol.* **117,** 91–101 CrossRef Medline
38. Kasimova, M. A., Tewari, D., Cowgill, J. B., Ursuleaz, W. C., Lin, J. L., Delemotte, L., and Chanda, B. (2019) Helix breaking transition in the S4 of HCN channel is critical for hyperpolarization-dependent gating. *Elife* **8,** e53400 CrossRef Medline
39. Craven, K. B., and Zagotta, W. N. (2004) Salt bridges and gating in the COOH-terminal region of HCN2 and CNGA1 channels. *J. Gen. Physiol.* **124,** 663–677 CrossRef Medline
40. Puljung, M. C., DeBerg, H. A., Zagotta, W. N., and Stoll, S. (2014) Double electron-electron resonance reveals cAMP-induced conformational change in HCN channels. *Proc. Natl. Acad. Sci. U.S.A.* **111,** 9816–9821 CrossRef Medline
41. Wainger, B. J., DeGennaro, M., Santoro, B., Siegelbaum, S. A., and Tibbs, G. R. (2001) Molecular mechanism of cAMP modulation of HCN pacemaker channels. *Nature* **411,** 805–810 CrossRef Medline
42. Gianulis, E. C., Liu, Q., and Trudeau, M. C. (2013) Direct interaction of eag domains and cyclic nucleotide-binding homology domains regulate deactivation gating in hERG channels. *J. Gen. Physiol.* **142,** 351–366 CrossRef Medline